Dynamic mechanical analysis of (Ca,Sr)AlSiN3

Eu2+ phosphor/silicone composites aged under the temperature–humidity–sulfur coupled condition

Feng, Shuo; Jiang, Tao ; Chen, Wei; Fan, Xuejun; Zhang, Guoqi ; Fan, Jiajie

DOI
10.1109/ICEPT56209.2022.9873248

Publication date
2022

Document Version
Final published version

Published in
Proceedings of the 2022 23rd International Conference on Electronic Packaging Technology (ICEPT)

Dynamic mechanical analysis of (Ca,Sr)$AlSiN_3$:Eu^{2+} phosphor/silicone composites aged under the temperature–humidity–sulfur coupled condition

Shuo Feng
Academy for Engineering & Technology
Fudan University
Shanghai, China
21210860045@m.fudan.edu.cn

Tao Jiang
College of Mechanical and Electrical Engineering
Hohai University
Changzhou, China
jiangtao.hehai@foxmail.com

Wei Chen
Academy for Engineering & Technology
Fudan University
Shanghai, China
chenw21@m.fudan.edu.cn

Xuejun Fan
Department of Mechanical Engineering
Lamar University
Beaumont, USA
xfan@lamar.edu

Guoqi Zhang
EEMCS Faculty
Delft University of Technology
Delft, The Netherlands
g.q.zhang@tudelft.nl

Jiajie Fan*
Academy for Engineering & Technology, Fudan University, Shanghai, China

State Key Laboratory of Applied Optics, Changchun Institute of Optics, Fine Mechanics and Physics, Chinese Academy of Sciences, Changchun, China

Fudan Zhangjiang Institute, Shanghai, China
jiajie_fan@fudan.edu.cn

2022 23rd International Conference on Electronic Packaging Technology (ICEPT) | 978-1-6654-9905-7/22/$31.00 ©2022 IEEE | DOI: 10.1109/ICEPT56209.2022.9873248

***Abstract*—As a core packaging material of light color conversion, phosphor/silicone composite plays an indispensable role in light emitting diode (LED) packaging. At present, commercial LED packages mainly use blue LED chips to stimulate Yttrium Aluminum Garnet (YAG) yellow phosphor to reach a white color. However, (Ca,Sr)$AlSiN_3$:Eu^{2+} (CSASN) red phosphor is often added to improve the color-rendering performance given the absence of red light emission spectrum. However, inevitably harsh working conditions can induce the degradation of CSASN red phosphor, which will directly influence the mechanical properties of its silicone composites and challenge the reliability of its LED packaging. In this study, the coupling effects of temperature–humidity–sulfur on the mechanical degradation of CSASN phosphor/silicone composites were considered. The prepared CSASN phosphor/silicone test samples were first aged under high-temperature, high-humidity, and high-sulfur conditions. A series of dynamic mechanical analysis tests were then conducted to qualitatively evaluate their mechanical properties. Finally, the dynamic tension process and interfacial cracking of CSASN phosphor/silicone composites were simulated by using finite element analysis with cohesive modeling. The results showed that: (1) under coupled aging conditions, the mechanical properties of the phosphor/silicone composite decreased due to the reaction of phosphor with sulfur, water, and oxygen; (2) crack initiation and propagation were most likely to occur at the edge of the crack perpendicular to the tensile direction. The debonding of particles with silicone rather than the fracture of phosphors was one of the main aspects resulting in failure mechanisms; (3) the highly concentrated and localized phosphor in the silicone matrix and the irregular shape and arrangement of phosphor particles generated cracks in the phosphor/silicone composite.**

Keywords—LED packaging; phosphor/silicone composites; (Ca,Sr)$AlSiN_3$:Eu^{2+}; dynamic mechanical analysis; temperature–humidity–sulfur coupled effect

I. INTRODUCTION

Light emitting diodes (LEDs) have become an important next-generation environmentally friendly solid-state lighting sources on account of their high efficiency, energy saving, and long life span [1][2]. LED packages are widely applied in indoor and outdoor lighting, liquid crystal backlight (LCD), automobile headlights, and other fields [3]. However, harsh working environments pose a great challenge to the reliability of LED packages [4]. As the key material for light conversion in white LED packaging, the phosphor/silicone composites play an extremely crucial role in determining the package level luminous efficiency, color rendering, and reliability [5][6].

At present, most commercial white LED packages mainly use blue LED chip to stimulate Yttrium Aluminum Garnet (YAG) yellow phosphor to achieve its white color [7]. Although this kind of LED has high luminous efficiency, it can only obtain cold white light with low color rendering index (R_a < 80) and higher color temperature (CCT > 7000K) as it lacks red light emission [8]. Currently, $CaAlSiN_3$:Eu^{2+} (CASN) red phosphor and its derivatives are always used to enhance the color rendering performance of white LEDs. However, these red phosphors are extremely sensitive to the inevitable harsh working conditions, *i.e.*, high temperature and high humidity [9], which affect the optical and mechanical properties of phosphor/silicone composites directly [10].

Recent studies have investigated the effect of aging on silicone, CASN serious phosphor, and their composites. For example, Kochanke *et al.* [11] applied 85°C/85%RH condition to age a silicone adhesive, and employed Fourier transform infrared spectroscopy (FTIR) to explore its degradation mechanism in bulk material properties. Chen *et al.* [12] studied the optical and mechanical properties of silicone encapsulant aged under a high-sulfur condition, which showed that the sulfhydryl (-SH) group, which was formed during vulcanization, deteriorated the overall performance of the silicone encapsulant. Cai *et al.* [13] analyzed the optical and mechanical degradation mechanisms of CSASN silicone/phosphor under high-temperature, high-humidity, and high-sulfur conditions with FTIR and finite elemental analysis (FEA) simulations. Cui *et al.* [14] simulated the hydrolysis process of CASN phosphor and its adhesion effects onto silicone interface with Density Functional Theory (DFT) simulations. The results revealed that the moisture diffusion of the CASN phosphor interfaces resulted in a decrease in

light output, such that the hydrolysis reaction of phosphor would increase its adhesion on the silicone interface.

Furthermore, the mechanical failure of phosphor/silicone composites may cause delamination, cracks, or even fracture of the LED packaging, which is a great challenge to the reliability of its packaging. In this paper, the coupling effect of temperature–humidity–sulfur on the mechanical degradation of composites was investigated. Firstly, the CSASN phosphor/silicone composites were aged under different conditions, *i.e.*, high-temperature, high-humidity, and varying sulfur concentrations. A series of dynamic mechanical analysis (DMA) experiments were then conducted to qualitatively compare their aging mechanisms by extracting the variation tendencies of their mechanical properties. Finally, the dynamic tension process and interfacial cracking of the CSASN phosphor/silicone composites were investigated by using finite element analysis (FEA) with cohesive modeling.

II. Sample Preparation and Experiments

A. Sample preparation

The preparation process of the phosphor/silicone composite samples can be segmented into the following steps: First, 10% mass fraction of CSASN red phosphor (R6535) was mixed with silicone (KJC-1200 A/B) equivalently. The material properties of phosphor and silicone are listed in Table I. Next, the mixture was stirred for about 15 min with a stirring rod and using a vacuum tank to remove the bubbles. The air pressure was set at approximately 6×10^{-2} Pa. The uncured mixture was then poured into the mold to eliminate the bubbles again. Furthermore, the mold with uncured mixture was cured under 100°C for 4 h. In the end, the cured silicone/phosphor composites were cut into a "dumbbell" shape with the size defined by the ASTMD1708 standard, as shown in Fig. 1.

TABLE I Material properties of Phosphor and Silicone

Materials	Density (10^3 kg/mm^3)	Poisson's ratio	Young's Modulus (MPa)
Silicone	1.04×10^{-9}	0.48	3.10
CSASN phosphor	3.10×10^{-9}	0.28	335000

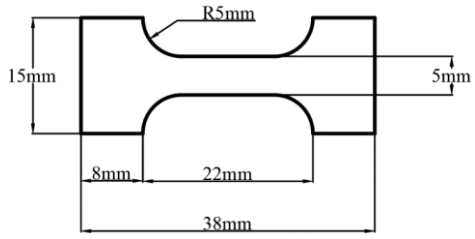

Fig. 1. Size of the silicone/phosphor composite test sample.

B. Aging experiment and mechanical test

In order to simulate the harsh usage conditions of LED packages, we designed four groups of aging experimental conditions, as shown in Table II — Group 1: High temperature (100°C); Group 2: High temperature and high humidity (100°C+100%RH); Group 3: High temperature and high sulfur (100°C+Sulfur); and Group 4: High temperature, high humidity and high sulfur (100°C+100%RH+Sulfur). The aging duration was set as 1008 h.

TABLE II The Quantities of Each Group

Group No.	Aging Conditions	Sample size
1	100°C	4
2	100°C+100%RH	6
3	100°C+Sulfur	6
4	100°C+100%RH+Sulfur	6

The DMA tests were conducted on the CSASN phosphor/silicone composites by using IBTC-5KST (Care measurement and control, China), as shown in Fig. 2. The symmetrical biaxial tensile loading mode was adopted. In order to ensure that the central position of the loaded specimen remained unchanged, the sample was fixed at both ends with a chuck at a loading rate of 1.5×10^{-3} m/s. The sample was stretched at a specific uniform speed and compressed to the original at a uniform speed when the load reached 12N. Through this low strain rate cyclic tension, the sample's fracture cycles, Young's modulus, and other mechanical parameters were obtained.

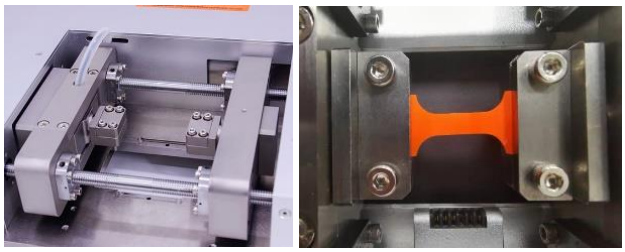

Fig. 2. CSASN phosphor/silicone composite test sample in an IBTC-5KST DMA tester.

III. Experimental Results and Discussion

A. Fracture Cycles

The cyclic tensile tests of each group's samples were carried out based on the experimental scheme and the maximum load was 12N until fracture. The fracture cycles of samples under various aging conditions are representatively shown in Fig. 4. Under the temperature–humidity–sulfur coupled condition, the fracture cycle No. of CSASN phosphor/silicone composite significantly increased because the sulfur reacted with moisture as hydrogen sulfide permeated and reacted with silicone and phosphor.

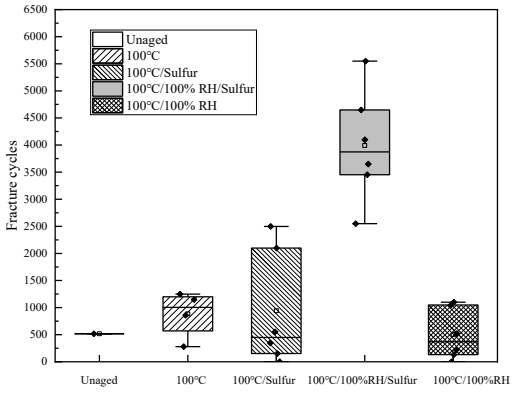

Fig. 4. Fracture cycles of the CSASN phosphor/silicone composite test samples aged under different conditions.

B. Young's Modulus

Young's modulus is the ratio of the axial strain to axial stress and is used to characterize the tensile or compressive

strength of a material. The calculation formula of axial strain is shown as follows:

$$E = \frac{\sigma_{a2}-\sigma_{a1}}{\varepsilon_{a2}-\varepsilon_{a1}}, \quad (1)$$

where σ_{a2} and σ_{a1} respectively define the axial stresses corresponding to any two points near the straight-line segment; and ε_{a2} and ε_{a1} are the axial strains corresponding to σ_{a2} and σ_{a1}, respectively.

As shown in Fig. 5, the Young's modulus of the aged samples decreased to a certain extent under different conditions. Under the high temperature and high humidity (100°C/100%RH) condition, the Young's modulus of the samples increased slightly. It is speculated that the phosphor hydrolyzed and the surface adhesion of the material increased. In comparison, under the temperature–humidity–sulfur coupled condition (100°C+100%RH+Sulfur), the Young's modulus of the samples significantly decreased. The hydrolysis reaction raised the Young's modulus and lowered tensile fracture cycle, whereas the vulcanization reaction resulted in a decrease in the Young's modulus and an increasement in the tensile fracture cycle.

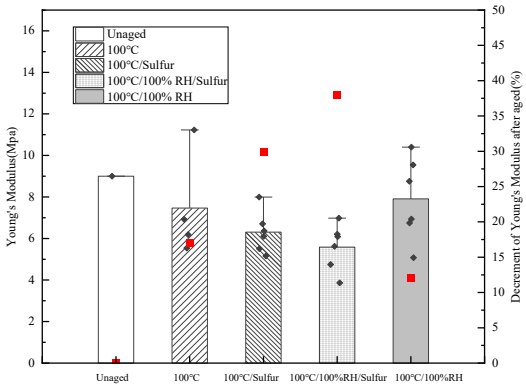

Fig. 5. Young's modulus of the samples aged under different conditions.

IV. Cohesion Modeling and FEA Simulation

The cohesion model is always used to describe the mechanical behavior of interface, which was originally proposed by Dugdale [15] and Barenblatt [16] to figure out the elastic-plastic fracture of ductile metals. In recent years, the cohesion model has been widely applied to investigate the transformation of brittle materials to composites, metals, polymers, and functionally graded materials, especially under specific engineering problems, such as dynamic crack propagation, crack initiation, and interfacial debonding of composites. In this paper, the FEA with ABAQUS was used to simulate the tensile fracture of the phosphor/silicone composite.

A. Cohesion Modeling

The CSASN red phosphor particles and its particle size distribution are shown in Fig. 6. The scanning electron microscopy (SEM) image shows irregular shapes and distributions of the phosphor particles, similarly to what is observed in an irregular polygon. However, most previous researches mainly used ellipse [13] or sphere models [17] to simulate phosphor particles, without considering its irregular shape. In order to obtain the material stress concentration range, internal fracture trend, and other microscopic mechanical properties, the present study proposed a cohesive model describing the bonding of phosphor to silicone.

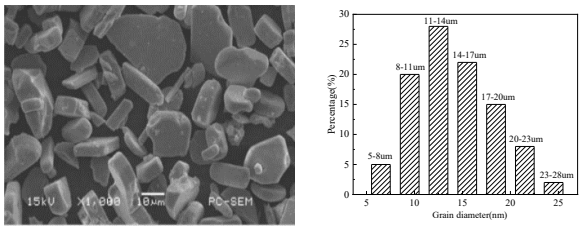

Fig. 6. CSASN red phosphor particles and its particle size distribution.

A 2D silicone model with a size of 1000 μm × 1000 μm was established in advance. The phosphor particles were generated with random irregular polygon in Python, which can generate a certain mass fraction of phosphor/silicone composite model. As a result, the produced polygonal diameter could be controlled independently. To ensure randomness, the boundary between phosphor and silicone was controlled under a non-interference mode. In order to fit with the particle size distribution shown in Fig. 6, four radius sizes, *i.e.* 5-11 μm, 11-14 μm, 14-17 μm, and 17-28 μm, were set.

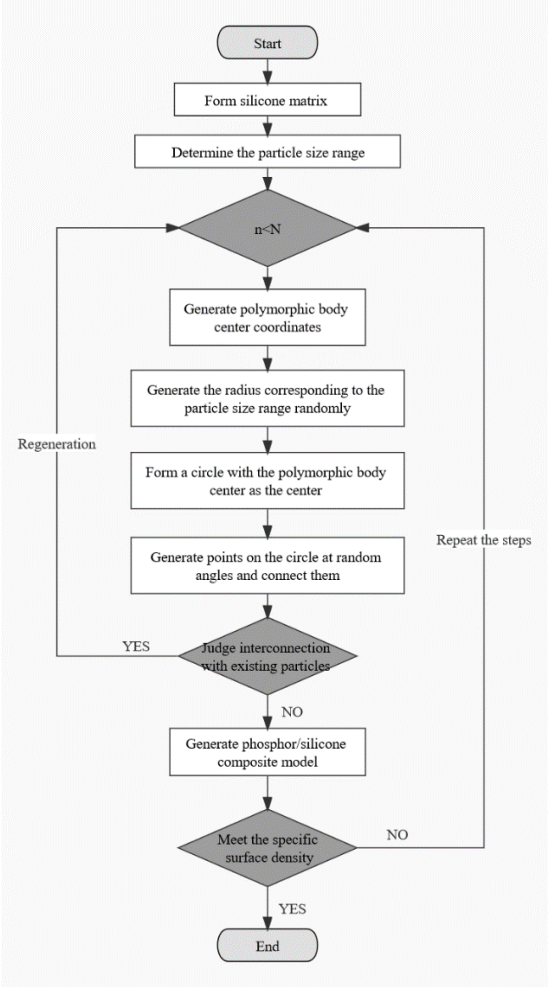

Fig. 7. Flowchart of 2D modeling of CSASN phosphor/silicone composite.

The specific modeling flowchart is shown in Fig. 7, which is described as follows: First, the corresponding silicone matrix size was generated in ABAQUS. A randomly selected a point (x, y) was then selected as the center of the polygon in the base, from which the radius was randomly selected on the base of the particle size distribution. A series of random angles with the same number of random radii was then created to generate the corresponding number of column

random points. The points were arranged and connected according to the order of the angle, and the number of edges of the polygon were controlled by increasing or decreasing the array. If the particle did not intersect or overlap with the existing particle, the particle would be successfully released and proceeded to the next release. Otherwise, the release was relaunched. Finally, steps (2) ~ (5) were repeated until the total aggregate content was reached to determine if the area density requirements were satisfied. The corresponding 2D model was successfully established, as shown in Fig. 8.

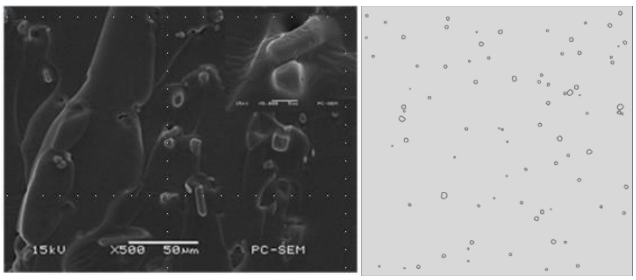

Fig. 8. SEM image and 2D model of the CSASN phosphor/silicone composite (1000 μm × 1000 μm).

The definition of material properties is an important part of cohesion simulation. The material properties such as phosphor and silicone density as well as the Young's modulus used in this paper are listed in Table I. When the cohesion model was used to simulate the damage of the material, the failure of the material was determined according to the damage initiation criterion. Initial damage indicated material stiffness degradation, and the initial condition of degradation were set as the stress and strain values upon reaching the damage limit [18]. The Maximum Nominal Stress Criterion (Maxs Damage) was used to analyze the bonding and tension of composites, as follows:

$$MAX\{\frac{\sigma_n}{N_{max}}, \frac{\sigma_s}{S_{max}}, \frac{\sigma_t}{T_{max}}\} = 1, \qquad (2)$$

where σ_n defines the nominal stress; σ_s is nominal stress in the first direction; σ_t is nominal stress in the second direction; and $N_{\max}$, $S_{\max}$, and $T_{\max}$ refer to the nominal damage stress conditions in corresponding direction. This damage initiation criteria means that when any nominal stress reached 1, nominal damage stress ensued and the damage began.

In this paper, the Maxs Damage was used and the type of damage evolution in the dynamic tension simulation was based on energy as well as the behavior of the mixed mode following the power law. In order to achieve better convergence, the damage stability viscosity coefficient was set to 0.05. The nominal damage stress and the maximum damage stress were set up to 0.2 MPa. To increase the accuracy of the calculation, the composite was divided into artificial meshes. To fit the irregular phosphor particles, a free mesh division was selected. The quadrilateral element was inserted in the cohesive seams at the edge of the mesh. In order to better fit the DMA tensile experiment, this simulation adopted the dynamic displacement loading to stretch both ends of the model in horizontal direction (x-axis) and vertical direction (y-axis), which produced an obvious interface separation between phosphor and silicone.

B. Cohesion simulation results

The biaxial tensions of the x-axis and y-axis were simulated in ABAQUS. The simulation results of the phosphor/silicone composites and stress distribution near phosphor particles are shown in Fig. 9. Under the dynamic tension, the silicone substrate was more prone to deformation as the phosphor's Young's modulus was higher as compared to the phosphor material. During the tension process, when the stress distribution at the intersection of the phosphor particles and silicone boundary was more concentrated, greater stress in a portion of the silicone matrix produced more obvious separation from the phosphor powder. The stress distribution of silicone was more concentrated at both sharp ends. The simulation results fit the experimental results to a certain extent. For samples under same aging conditions with significant difference in mechanical properties, the difference was on account of the highly localized and concentrated phosphor dispersion in silicone. Moreover, the irregular shape and arrangement of the phosphor particles may have also have affected this. In addition, the edge of the crack, which was perpendicular to the direction to extrude, was identified around the debonding particle region as well, indicating that the crack was most probably to form and propagate in this section. The simulation results showed that the debonding between phosphor particles and silicone matrix rather than the fracture of the phosphor was one of the main aspects resulting in failure mechanisms of the composites.

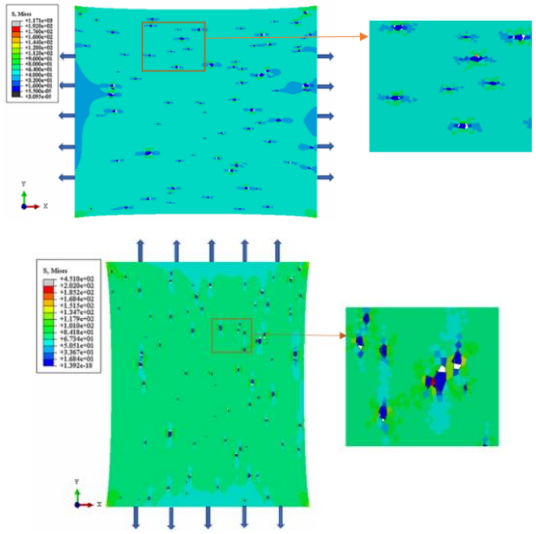

Fig. 9. Biaxial simulation results and stress distribution near the phosphor particles along the x-axis and y-axis.

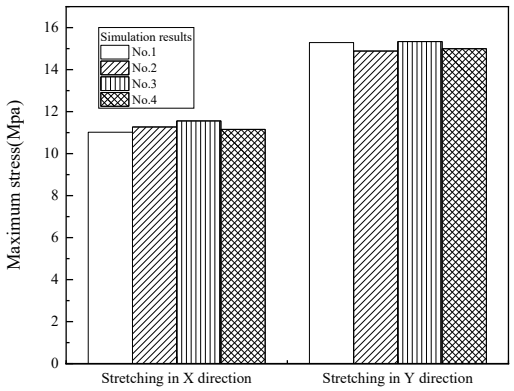

Fig. 10. Simulation results of maximum stress at different tensile directions.

The experimental process of uniaxial bidirectional tension on the x-axis and y-axis was simulated four times for each group. According to the results in Fig. 10, all simulation stress results of each group were basically the same, though

obvious differences were observed in the stress distribution on the different axes.

C. Discussion on experiments and simulations

Referring to [14], the adhesion of silicone molecular on the pristine CaAlSiN3 [0 1 0] showed weak physisorption via Van der Waals (vdW) interaction, as shown in Fig. 11.

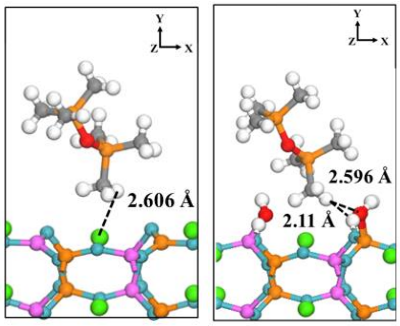

Fig. 11. van der Waals interconnection between silicone and CASN phosphor before and after hydrolysis [14].

In addition, the formation of interfacial hydrogen bond after hydrolysis [14] and the formation of hydrogen sulfide after vulcanization [12] produced worsened silicone mechanical properties. Through the simulation results, the interface delamination between the phosphor granules and silicone successively proceeded in the same dimension, which led to crack initiation or fracture of the sample. Under high-temperature aging, the cross-linking degree of silicone increased while the fracture strain decreased. These material property changes may be a result of the consumption of excess hydrosiloxane (Si-H) groups [11]. Under high-temperature and high-humidity conditions, the phosphor hydrolyzed, thus allowing the moisture to interfere with the accumulation of adhesion, which was very unfavorable for adhesion [19]. Under high-temperature and high-sulfur conditions, the silicone protected phosphor particles from the vulcanization reaction. However, with the help of moisture, the generated hydrogen sulfide permeated and reacted with silicone and phosphor, which significantly deteriorated the mechanical properties.

V. Conclusion

In this paper, the coupling effect of temperature, humidity, and sulfur on the mechanical and interfacial properties of CSASN phosphor/silicone composites were investigated through both experimental and simulation analyses. The macroscopic behavior of the aged composites was characterized by dynamic tensile test, and a cohesion model was established to simulate their tensile and interfacial delamination behaviors. The results show that: (1) under coupled temperature- humidity-sulfur condition, both the mechanical properties and fracture strain of the phosphor/silicone composite decreased due to the reaction of phosphor with sulfur, water, and oxygen. The hydrolysis reaction led to an increase in the Young's modulus and a decrease in the tensile fracture cycle. In comparison, the vulcanization reaction resulted in the opposite results; (2) crack initiation and propagation were most likely to occur at the edge of crack perpendicular to tensile direction. The debonding of phosphor particles with silicone rather than the fracture of phosphors was one of the main aspects resulting in failure mechanisms; (3) the highly concentrated and localized phosphor dispersion in the silicone and the irregular shape and arrangement of phosphor particles resulted in crack propagation. Consequently, in order to enhance the service lifespan of LED packaging under harsh working conditions, phosphors with uniform particle sizes and thermal-moisture-sulfur stabilities are suggested. Nevertheless, high humidity and sulfur conditions should be avoided in the working environment.

Acknowledgments

The work described in this paper was partially supported by the National Natural Science Foundation of China (51805147), Shanghai Science and Technology Development Foundation (21DZ2205200), State Key Laboratory of Applied Optics (SKLAO2022001A01), and Shanghai Pujiang Program (2021PJD002).

References

[1] R. D. Dupuis and M. R. Krames, "History, development, and applications of high-brightness visible light-emitting diodes," *Journal of Lightwave Technology,* vol. 26, no. 9-12, pp. 1154-1171, May-Jun 2008.

[2] S. Pimputkar, J. S. Speck, S. P. DenBaars, and S. Nakamura, "Prospects for LED lighting," *Nature Photonics,* vol. 3, no. 4, pp. 179-181, Apr 2009.

[3] P. J. Yadav, C. P. Joshi, and S. V. Moharil, "Two phosphor converted white LED with improved CRI," *Journal of Luminescence,* vol. 136, pp. 1-4, Apr 2013.

[4] M.-H. Chang, D. Das, P. V. Varde, and M. Pecht, "Light emitting diodes reliability review," *Microelectronics Reliability,* vol. 52, no. 5, pp. 762-782, 2012/05/01/ 2012.

[5] M. Meneghini, A. Tazzoli, G. Mura, G. Meneghesso, and E. Zanoni, "A Review on the Physical Mechanisms That Limit the Reliability of GaN-Based LEDs," *Ieee Transactions on Electron Devices,* vol. 57, no. 1, pp. 108-118, Jan 2010.

[6] C. Damian, E. Espuche, and M. Escoubes, "Influence of three ageing types (thermal oxidation, radiochemical and hydrolytic ageing) on the structure and gas transport properties of epoxy-amine networks," *Polymer Degradation and Stability,* vol. 72, no. 3, pp. 447-458, 2001 2001.

[7] Y. G. Yoon, J. H. Kang, I. H. Jang, S. I. Chan, and J. S. Jang, "Conclusion of the accelerated stress conditions affecting phosphor-converted LEDs using the fractional factorial design method," *Microelectronics Reliability,* vol. 53, no. 9-11, pp. 1519-1523, Sep-Nov 2013.

[8] R. Liu, H. He, X. Huang, Y. Hu, Y. Liu, and W. Zhuang, "New Progress in Study and Application on Phosphors for White LED," *Semiconductor Technology,* vol. 37, no. 3, pp. 221-227, 2012, Art no. 1003-353x(2012)37:3<221:Bglygf>2.0.Tx;2-u.

[9] Y. Pan *et al.*, "Investigation of Mechanical Properties of Silicone/Phosphor Composite Used in Light Emitting Diodes Package," *Polymers,* vol. 10, no. 2, Feb 2018, Art no. 195.

[10] X. Luo, B. Wu, and S. Liu, "Effects of Moist Environments on LED Module Reliability," *Ieee Transactions on Device and Materials Reliability,* vol. 10, no. 2, pp. 182-186, Jun 2010.

[11] A. Kochanke, K. Kraemer, C. Ueffing, and A. Hartwig, "Influence of high-temperature and high-humidity aging on the material and adhesive properties of addition curing silicone adhesives," *International Journal of Adhesion and Adhesives,* vol. 111, Dec 2021, Art no. 102980.

[12] W. Chen *et al.*, "Sulfur-Rich Ageing Mechanism of Silicone Encapsulant Used in LED Packaging: An Experimental and Molecular Dynamic Simulation Study," *Frontiers in Materials,* vol. 9, Feb 28 2022, Art no. 819294.

[13] W. Cai, T. Jiang, and J. Fan, " Coupling effects of thermal-humidity-sulfur aging on mechanical properties of (Ca,Sr)AlSiN3:Eu2+ phosphor/silicone composites with experimental and numerical interpretation ," *Optical Materials,* vol. 128, Jun 2022, Art no. 112384.

[14] Z. Cui, J. Fan, H. J. van Ginkel, X. Fan, and G. Zhang, "The interface adhesion of CaAlSiN3: Eu2+ phosphor/silicone used in light-emitting diode packaging: A first principles study," *Applied Surface Science,* vol. 510, Apr 30 2020, Art no. 145251.

[15] D. S. Dugdale, "Yielding of Steel Sheets Containing Slits," *Journal of the Mechanics and Physics of Solids,* vol. 8, no. 2, pp. 100-104, 1960 1960.

[16] G. I. Barenblatt, "Citation Classic - The Mathematical - Theory of Equilibrium Cracks in Brittle-Fracture," *Current Contents/Engineering Technology & Applied Sciences,* no. 42, pp. 20-20, 1983 1983.
[17] H. M. Inglis, P. H. Geubelle, K. Matous, H. Tan, and Y. Huang, "Cohesive modeling of dewetting in particulate composites: micromechanics vs. multiscale finite element analysis," *Mechanics of Materials,* vol. 39, no. 6, pp. 580-595, Jun 2007.
[18] W. Jiang, H. Zou, Y. Xia, and Y. Zhou, "Effect of Vertical Cracks of Alumina Coating on Interface Failure under Thermal Load," *Surface Technology,* vol. 48, no. 1, pp. 30-36, 2019, Art no. 1001-3660(2019)48:1<30:Yhltcc>2.0.Tx;2-7.
[19] S. Ito, N. Hirai, and Y. Ohki, "Changes in mechanical and dielectric properties of silicone rubber induced by severe aging," *Ieee Transactions on Dielectrics and Electrical Insulation,* vol. 27, no. 3, pp. 722-730, Jun 2020.